JOURNAL OF GEOPHYSICAL RESEARCH, VOL. 114, A10315, doi:10.1029/2009JA014460, 2009

Causal link of the wave-4 structures in plasma density and vertical plasma drift in the low-latitude ionosphere

T.-W. Fang,[1,2] H. Kil,[3] G. Millward,[4] A. D. Richmond,[1] J.-Y. Liu,[2] and S.-J. Oh[5]

Received 13 May 2009; revised 10 July 2009; accepted 14 August 2009; published 23 October 2009.

[1] We investigate the annual and local time variations of the wave-4 structures in the plasma density and vertical drift in the low-latitude *F* region by analyzing the measurements from the first Republic of China satellite (ROCSAT-1) and conducting simulations with the Global Ionosphere and Plasmasphere (GIP) model. The GIP model uses apex magnetic coordinates with International Geomagnetic Reference Field (IGRF) for magnetic field, neutral wind from HWM-07, and thermospheric parameters from the NRLMSISE-00 model. In order to understand how the vertical drifts relate to the longitudinal structure of the topside ionosphere, we apply the equatorial vertical drifts observed from ROCSAT-1 to drive the GIP model. The model well reproduces the longitudinal structure in electron density, and the magnitudes of electron density are comparable with ROCSAT-1 measurement at 600 km. The ROCSAT-1 observations of the vertical drift and plasma density show maximum amplitudes of their wave-4 components in July–September and minimum amplitudes in December–February. An eastward shift of the wave-4 components with increasing local time is observed in both the density and the vertical drift. The GIP model density showed similar annual and local time variations of the wave-4 component. Since the model uses the observed equatorial vertical $\mathbf{E} \times \mathbf{B}$ drift as an input, the results indicate the vertical drifts are essential in the formation and evolution of the longitudinal wave-4 density structure. The amplitude of the eastward propagating diurnal tide (DE3) at 110 km shows similar annual and local time variations as the *F* region parameters, supporting the link between the DE3 tide, vertical $\mathbf{E} \times \mathbf{B}$ drift, and *F* region plasma density on a global scale.

Citation: Fang, T.-W., H. Kil, G. Millward, A. D. Richmond, J.-Y. Liu, and S.-J. Oh (2009), Causal link of the wave-4 structures in plasma density and vertical plasma drift in the low-latitude ionosphere, *J. Geophys. Res.*, *114*, A10315, doi:10.1029/2009JA014460.

1. Introduction

[2] Extensive studies in recent years, through satellite observations [e.g., *England et al.*, 2006; *Immel et al.*, 2006, 2009; *Kil et al.*, 2007, 2008; *Lin et al.*, 2007a, 2007b; *Liu and Watanabe*, 2008; *Lühr et al.*, 2007, 2008, *Scherliess et al.*, 2008; *Wan et al.*, 2008] and model simulations [e.g., *Hagan et al.*, 2007; *Jin et al.*, 2008; *Oh et al.*, 2008], reveal that solar thermal tides excited in the troposphere can induce longitudinal variability in the low-latitude ionospheric *F* region through ionospheric electrodynamic processes. *Hagan et al.* [2007] used the National Center for Atmospheric Research Thermosphere-Ionosphere-Mesosphere-Electrodynamics General Circulation Model (TIME-GCM) with lower boundary forcing from the Global Scale Wave Model (GSWM) to demonstrate that a wave number-4 longitudinal variation for a fixed local time is due to the modulation of vertical equatorial plasma drifts in the *F* region through the dynamo action of the eastward propagating diurnal tide of wave number 3 (DE3). Numerical simulations by *Jin et al.* [2008] confirmed this. *Oh et al.* [2008] used the vertical drift from the first Republic of China satellite (ROCSAT-1) during equinox as an input to drive the SAMI2 model (Sami2 is Another Model of the Ionosphere [*Huba et al.*, 2000]) and could reproduce the wave-4 structure in the plasma density observed by ROCSAT-1. These investigations demonstrate that longitudinal structure in the ionosphere may provide evidence of tropospheric effects on the ionosphere, but the direct link between the global vertical $\mathbf{E} \times \mathbf{B}$ drift and the plasma longitudinal structure and annual variation of their causal link have not yet been examined in detail.

[3] Models based on physical equations, observations (empirical), and data assimilation can aid us in understanding the causal mechanisms of different phenomena occurring in the thermosphere and ionosphere. In this study, we further investigate the link between the DE3 tide, vertical drift, and plasma density by analyzing satellite observation

[1]High Altitude Observatory, National Center for Atmospheric Research, Boulder, Colorado, USA.
[2]Institute of Space Science, National Central University, Jhongli City, Taiwan.
[3]Johns Hopkins University Applied Physics Laboratory, Laurel, Maryland, USA.
[4]Laboratory for Atmospheric and Space Physics, University of Colorado at Boulder, Boulder, Colorado, USA.
[5]Space Environment Laboratory, Inc., Seoul, South Korea.

0148-0227/09/2009JA014460$09.00

data and performing model simulations. Our investigation focuses on the annual and local time variations of the wave-4 components in the plasma density and vertical plasma drift. The Global Ionosphere and Plasmasphere (GIP) model is suitable for this study since we can single out the response of the ionosphere to the input vertical drift. The development of a high-resolution equatorial vertical $\mathbf{E} \times \mathbf{B}$ drift model based on ROCSAT-1 observations [*Kil et al.*, 2009a] enables the investigation of the ionospheric response to the annual and local time variation of the wave-4 component in the vertical drift. We use this vertical drift model to replace the Scherliess and Fejer empirical vertical drift model [*Scherliess and Fejer*, 1999] originally taken in the GIP model for low-latitude $\mathbf{E} \times \mathbf{B}$ drifts. We apply the drift values above the magnetic equator for different longitudes and local times in different months and corresponding solar activity, and evaluate the effect of the vertical drift on the formation of the wave-4 density structure by comparing the GIP model simulation results with observations of the plasma density and vertical drift from ROCSAT-1. In section 2, we introduce the GIP model. In section 3 we present the local time, longitude, latitude, and altitude variations of the GIP model ionosphere. The GIP model ionosphere at 600 km is compared with the ROCSAT-1 observations. In section 4, we investigate the annual and local time variations of the wave-4 component in the plasma density and vertical plasma drift. Conclusions are given in section 5.

2. GIP Model Description

[4] The global Ionosphere Plasmasphere model (GIP) is a new modular Fortran-90 code which solves coupled equations of continuity, momentum and energy balance equations along the magnetic field line and calculates time-dependent ionospheric and plasmaspheric densities, temperatures, and velocities on a global, three-dimensional grid [*Millward et al.*, 2007]. The model uses the solar UV flux from *Torr and Torr* [1985] and the cross sections from *Torr and Torr* [1982]. The horizontal resolution in the low-latitude region is about 1° in latitude and 4.5° in longitude. In altitude, it covers the whole plasmasphere and gives information from 100 km to higher than 20,000 km. The modular construction allows for GIP to be easily coupled to any kind of background neutral atmospheric models. All of the necessary transformations, from the geographic/pressure coordinate systems favored by models of the neutral atmosphere to the magnetic field-aligned framework of the global ionosphere (and vice versa), are handled by sophisticated global ''interfaces'' contained within the GIP code itself. GIP is a further development arising from known deficiencies within the ionospheric component of the Coupled Thermosphere Ionosphere Plasmasphere model (CTIP) [*Millward et al.*, 2001]. CTIP utilized an offset-dipole model of the Earth's magnetic field. While effective up to a point, the dipole is an incomplete description for the actual terrestrial field. This leads to serious inaccuracies, most notably in the equatorial American and the South Atlantic sectors where the magnetic field deviates strongly from a dipole. To move beyond this dipole description, GIP utilizes a new Magnetic Apex coordinate system [*Richmond*, 1995] in which a global three-dimensional grid of magnetic field lines are created by tracing through the full International Geomagnetic Reference Field (IGRF). The resulting global grid contains all of the correct distortions and anomalies that characterize the actual terrestrial field. By using more realistic magnetic coordinates, the low-latitude ionosphere is greatly improved, since most plasma phenomena are controlled by the configuration of Earth's magnetic field. In addition, as mentioned above, GIP goes beyond CTIP by making the ionospheric/plasmasphere into a global module with interfaces for the input of background neutral parameters and the output of the calculated ionospheric parameters. This new modular approach allows for great flexibility of studies by allowing GIP to be coupled to any number of thermospheric models. *Fuller-Rowell et al.* [2008] developed the Integrated Dynamics through Earth's Atmosphere (IDEA) by coupling the Whole Atmosphere Model (WAM) to the GIP model to address the physical processes responsible for the impact of terrestrial weather on the upper atmosphere and ionosphere. In their study, the GIP model is the main module for plasma processes and electrodynamic calculations.

[5] In this study, we use the GIP model with empirical models providing the horizontal neutral wind, thermospheric parameters, and the equatorial vertical drifts. We retrieve the horizontal neutral wind from the Horizontal Wind Model (HWM-07) [*Drob et al.*, 2008], thermospheric densities and temperature from the Naval Research Laboratory Mass Spectrometer Incoherent Scatter Radar model (NRLMSISE-00) [*Picone et al.*, 2002], and the equatorial vertical drift from the model derived from ROCSAT-1 data [*Kil et al.*, 2009a].

3. Climatology of the GIP Model Ionosphere

[6] The GIP model simulations are performed for $F_{10.7} = 180$, using the vertical $\mathbf{E} \times \mathbf{B}$ drift model representative of moderately high solar activity ($130 < F_{10.7} < 200$) from the companion paper. The drifts are applied above the magnetic equator at each time step for the appropriate longitude and local time. The model ionospheric densities are obtained on day 15 of each month. In total we have 12 runs. After running the GIP model, we compare the simulated results with plasma density maps constructed from ROCSAT-1 observations. ROCSAT-1 operated from March 1999 to June 2004 at an altitude of 600 km, in a circular orbit with an inclination of 35 degrees [*Yeh et al.*, 1999]. For comparison of the model ionosphere with the observations, we process the ROCSAT-1 density data under the condition $F_{10.7} > 130$. Figure 1 (left) and Figure 1 (right) show the low-latitude density maps from the GIP model at 600 km and from ROCSAT-1 observations, respectively. The density maps from these two sources are shown at three local times (1100, 1500, and 2100 LT from the top to the bottom) in four seasons. Overall, the densities in the model results show consistently larger values than the observations. The disagreement is possibly due to the wide range of solar activity in the density observations and in the vertical drift data. Inaccuracies of the model EUV flux, neutral densities, or reaction rates may also contribute to the disagreement. Figure 1 shows that the equatorial ionization anomaly (EIA) [e.g., *Hanson and Moffett*, 1966; *Anderson*, 1973; *Bailey and Balan*, 1996] regions are limited within ±20°N magnetic latitude at 600 km altitude. But the latitude coverage

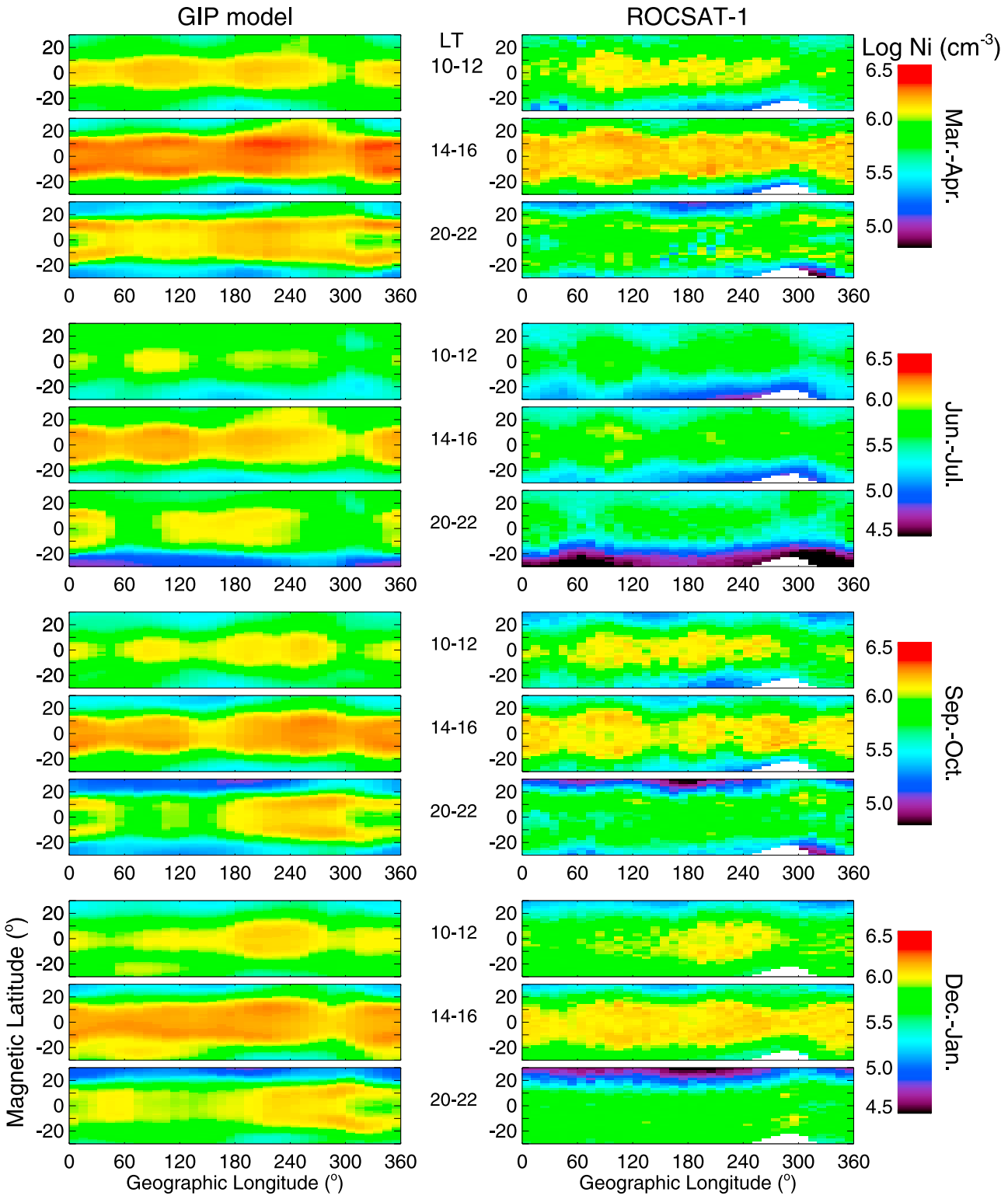

Figure 1. Comparison of the GIP and ROCSAT-1 densities at 600 km in three local times (1100, 1500, 2100 LT) and four seasons. The GIP model ionosphere is obtained for $F_{10.7}$ = 180. The ROCSAT-1 density is the mean density for $F_{10.7} > 130$.

of the EIA is slightly narrower in model simulation than in observation in the daytime. The longitudinal variation of the density shows good agreement between the GIP model and the ROCSAT-1 observations, especially during the daytime. The wave-like longitudinal density structure appears before noon and further intensifies in the afternoon. The premidnight longitudinal density structures in both the simulations and observations are significantly different from the density structure during the day.

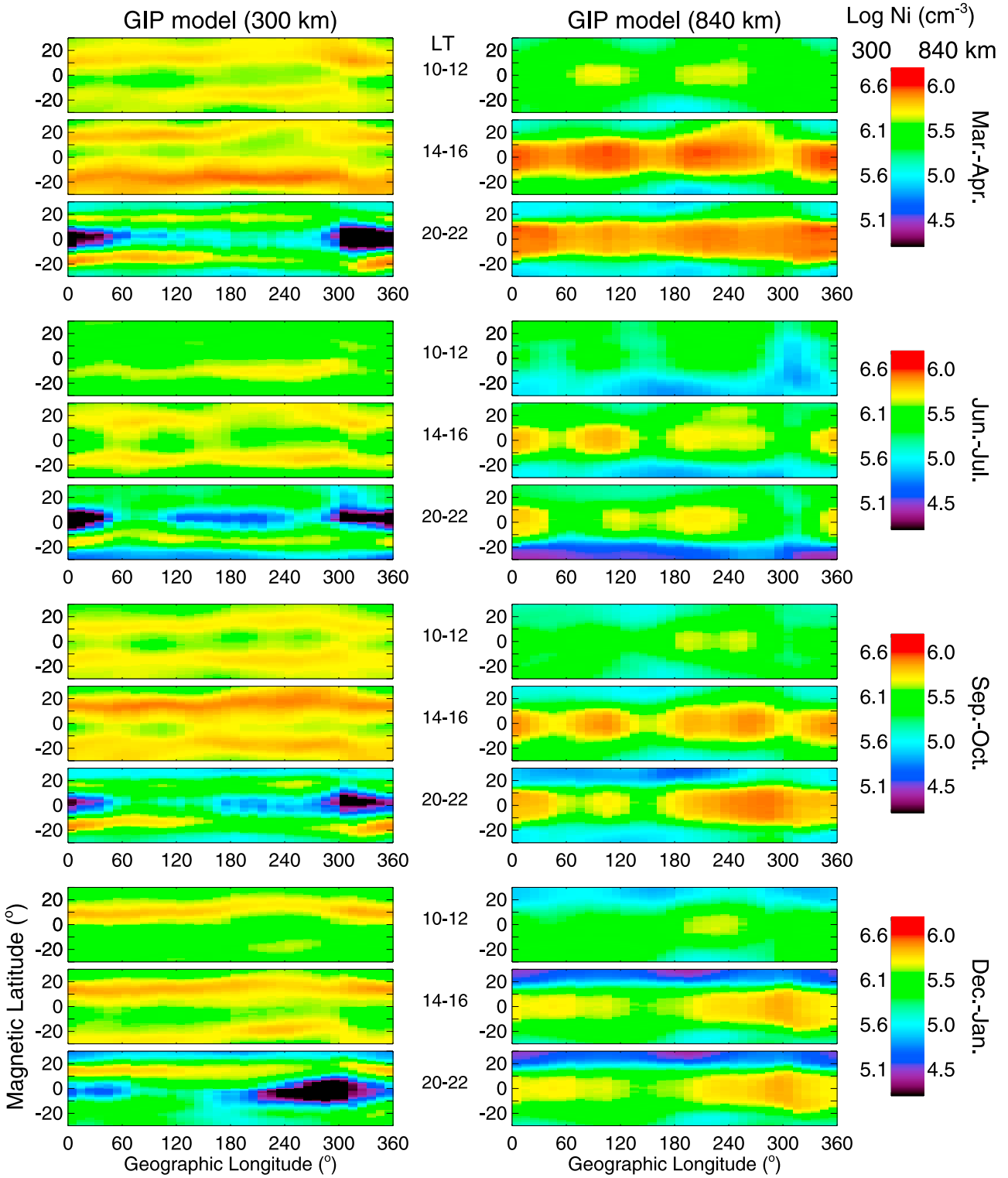

Figure 2. Comparison of the longitudinal density structure of the GIP model ionosphere at 300 km and 840 km at three local times (1100, 1500, 2100 LT) for four seasons. Note the use of different color scales at 300 km and 840 km.

[7] In the low-latitude topside ionosphere (600 km) neither the model nor the observations show distinguishable EIAs in the daytime. However, the shape of EIA is more evident at premidnight than during the day in both the model and observed ionosphere. The separation of the northern and southern EIAs at 2100 LT may indicate the significant role of the evening prereversal enhancement (PRE) in modifying the premidnight ionosphere. The large separation of the northern and southern EIAs in the equinoxes (March and September) is consistent with the

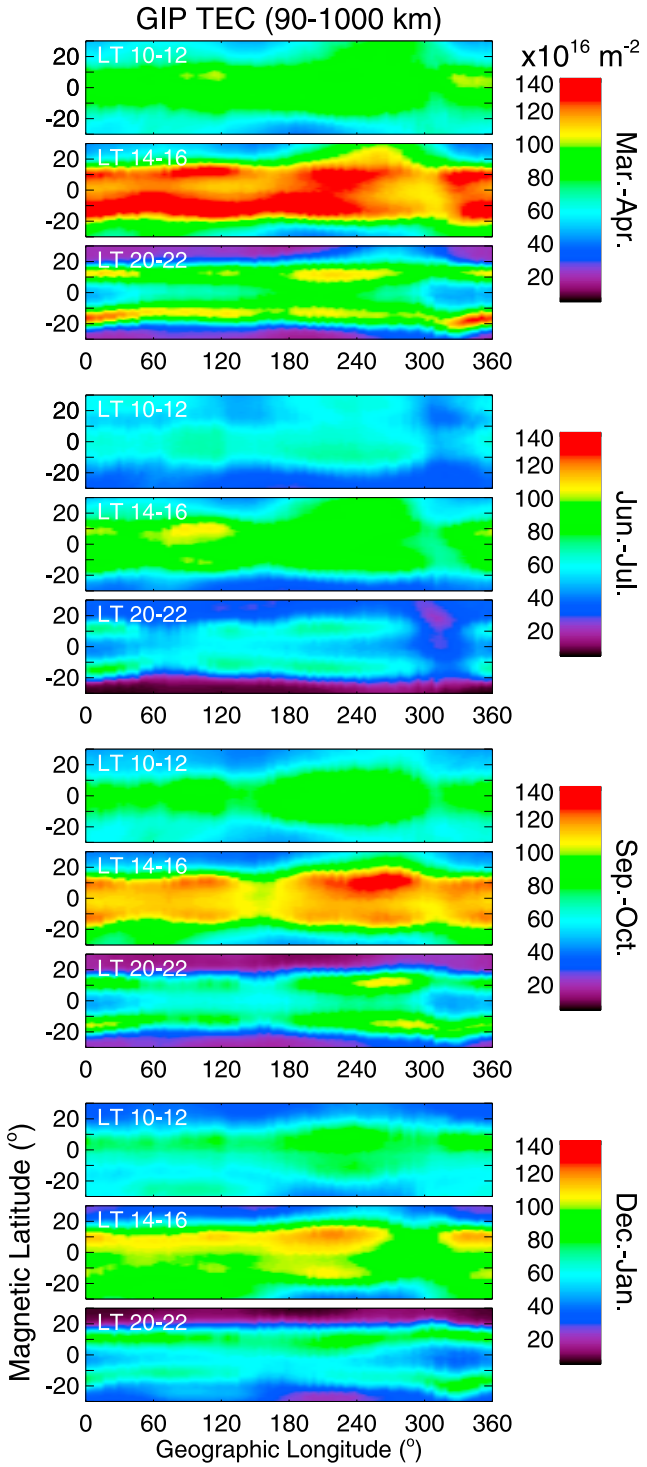

Figure 3. Simulated TEC from the GIP model at three local times (1100, 1500, 2100 LT) for four seasons.

occurrence of a pronounced PRE at most longitudes at equinox [*Kil et al.*, 2009b]. The daytime plasma density is quite symmetric about the magnetic equator in all seasons, in both the observed and model ionosphere. This result may indicate that plasma transport by the vertical $\mathbf{E} \times \mathbf{B}$ drift dominates the daytime density structure in the topside ionosphere. *Stolle et al.* [2008] pointed out that the typical response time of the EIA at 400 km to variations in the zonal electric field, as estimated from the strength of the equatorial electrojet, is 1–2 h. Our simulation results also find a response time of the density to the vertical drift less than 2 h (not shown here), although it depends on the altitude and local time, and on the specific density feature being examined. At night, besides the PRE, the interhemispheric wind may affect the ionospheric morphology.

[8] The ionospheric morphology can change significantly in altitude since the effects of neutral winds, neutral composition, and vertical $\mathbf{E} \times \mathbf{B}$ drift in the ionosphere all vary with altitude [e.g., *Kil et al.*, 2006]. The GIP model is capable of reproducing three-dimensional plasma density in the whole ionosphere and plasmasphere. In Figure 2, we show the GIP density simulation results at 300 km (left) and 840 km (right). The format of Figure 2 is the same as that of Figure 1. At 300 km, the EIA develops before noon and persists into the evening. Also, in contrast to the hemispheric symmetry in the topside, the plasma density (EIA) at 300 km shows significant hemispheric asymmetry. An interesting feature is that the density asymmetry reverses between the morning and afternoon at equinox. The hemispheric asymmetries at 1400–1600 LT are opposite in March–April and September–October. At December solstices, the peak electron density in the EIA in the winter hemisphere is more intense than that in the summer hemisphere. Observations of the altitudinal difference of the hemispheric plasma distribution were reported by *Kil et al.* [2006] and *Lin et al.* [2007c]. These studies suggested that the transequatorial neutral wind plays an important role in producing the hemispheric asymmetry. Our examination of the interhemispheric winds in the *F* region from HWM-07 showed that the transequatorial winds exist in all seasons. Since the EIA morphology is affected by neutral winds, the longitudinal wave-like structure may be less pronounced at 300 km compared to that in the topside ionosphere. The investigation of the source of the asymmetry is beyond the scope of this paper. We postpone this investigation to the future study. At 840 km, the longitudinal wave structure is similar to that at 600 km, but with a smaller magnitude. The formation of the wave structure at 840 km in the model ionosphere is consistent with the observations of the wave structure in plasma density [*Kil et al.*, 2008] and vertical $\mathbf{E} \times \mathbf{B}$ drift [*Hartman and Heelis*, 2007] at 840 km from Defense Meteorological Satellite Program (DMSP) spacecraft.

[9] The EIA morphology at the altitude of 300 km may not be directly compared with the EIA morphology in optical observations in space [*Immel et al.*, 2006; *Kil et al.*, 2008] since optical measurements reflect the peak density of the nighttime ionosphere. The comparison of the GIP model total electron content (TEC) with the optical observation will be adequate. Figure 3 shows the GIP TEC from 90 km to 1000 km in altitude. The format of Figure 3 is the same as that of Figure 2. The TEC plot reflects the plasma distribution near the *F* peak and the wave-4 structure appears much clearer in September–October compared to that in other seasons. The separation of the southern and northern EIAs can be identified in the TEC plots. At 1500 LT, the longitudinal morphology of the TEC agrees with the morphology of the modeled and observed density at the altitude of 600 km (Figure 1). The longitudinal wave structure in the GIP TEC is consistent with the morphology

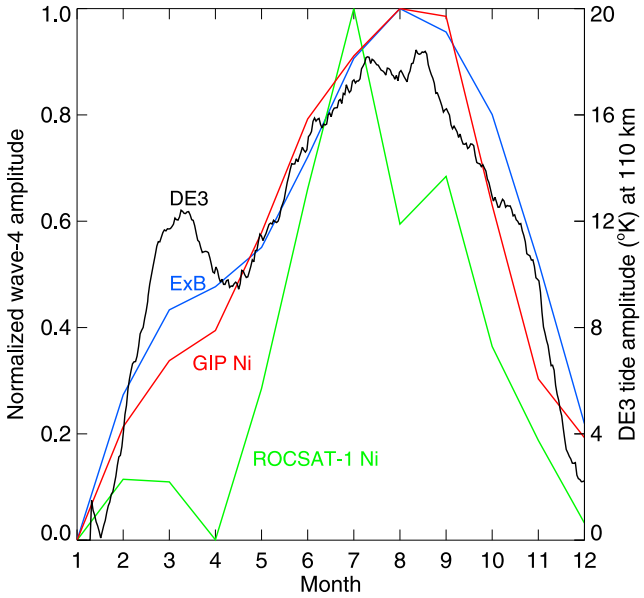

Figure 4. Annual variations of the DE3 tide (black), and the wave-4 components of the ROCSAT-1 vertical **E** × **B** drift (blue), GIP model density (red), and ROCSAT-1 density (green). The DE3 tide temperature is obtained from TIMED/SABER at 110 km in 2002. The wave-4 component of the vertical **E** × **B** drift is calculated using the mean ROCSAT-1 data between 1000–1400 LT under the condition $130 < F_{10.7} < 200$. The wave-4 component of the GIP model density was calculated at 1200 LT at 600 km under the condition $F_{10.7} = 180$. The wave-4 component of the ROCSAT-1 density is calculated using the data between 1000 and 1400 LT at 600 km under the condition $F_{10.7} > 130$. For the wave-4 density components of the GIP and ROCSAT-1 density we use the mean density from −20°N to 20°N magnetic latitude.

of the EIA [*Immel et al.*, 2006; *Kil et al.*, 2008; *Scherliess et al.*, 2008].

4. Annual and Local Time Variations of the Longitudinal Wave-4 Structure

[10] The formation of the four-peaked density structure in the EIA region and in the topside ionosphere has been confirmed by satellite observations [e.g., *Immel et al.*, 2006; *Kil et al.*, 2008]. The vertical plasma drift and equatorial electrojet observed above the magnetic equator during the day show longitudinal wave-4 structures which are similar to those in the daytime and evening plasma density [*England et al.*, 2006; *Kil et al.*, 2008; *Lühr et al.*, 2008]. The daytime vertical drifts in the equatorial region are controlled by the *E* region wind dynamo that is modulated by atmospheric tides. The nighttime electron density is affected by the daytime ionospheric morphology. As a result, similar longitudinal density structures are observed during the day and at night in some seasons [*Kil et al.*, 2008; *Scherliess et al.*, 2008]. The previous studies and our results shown in Figures 1–3 support the close link of the ionospheric wave-like density structure with the vertical drift. Here we provide further evidence of their causal link by examining the annual and local time variations of the wave-4 components in the vertical plasma drift and plasma density.

[11] Figure 1 and Figure 2 show that the wave-4 structures in the model and observation density are well developed near noon. Therefore, we calculate the mean vertical drift and density from the ROCSAT-1 data between 1000 and 1400 LT in each longitude and month. Then, since the separation of crests in the EIA region is not pronounced at 600 km, we calculated the mean density between −20°N and 20°N magnetic latitude for the ROCSAT-1 density. For the GIP model density, we choose 1200 LT and similarly calculate the mean density between −20°N and 20°N magnetic latitude. We extract the wave-4 component from the model and observed densities by Fourier analysis. Figure 4 shows the normalized annual variations of the wave-4 amplitudes from the ROCSAT-1 density (green curve), ROCSAT-1 vertical drift (blue curve), and GIP density at 600 km (red curve). The black curve shows the measurements of the peak temperature of the DE3 tide at 110 km in 2002 from the Sounding of the Atmosphere using Broadband Emission Radiometry (SABER) instrument on board the Thermosphere Ionosphere Mesosphere Energetics and Dynamics (TIMED) satellite [*Kil et al.*, 2008]. The annual variations of the amplitudes of the DE3 tide and of the wave-4 components in the vertical drift and density are consistent, showing their peaks in July–September. The correlation between the GIP density (red curve) and the input vertical **E** × **B** drift (blue curve) is remarkable. We note that other factors, such as neutral wind, neutral composition, and the displacement of the geographic and magnetic equators, also affect the *F* region morphology. The GIP simulation results are the consequence of these effects as well as the effect of the vertical drift.

[12] The horizontal wind measurements from the High Resolution Doppler Imager (HRDI) and the Wind Imaging Interferometer (WINDII) on board the Upper Atmosphere Research Satellite (UARS) show an annual variation of the amplitude of the DE3 tide [*Forbes et al.*, 2003]. The northward wind of the DE3 tide at 95 km observed by HRDI and WINDII has a minimum during May–September, whereas the zonal wind of the DE3 tide has a maximum in June–September. The observations of the horizontal wind from the TIMED Doppler Interferometer (TIDI) on board the TIMED satellite also show similar annual variations of the meridional and zonal velocities of the DE3 tide [*Oberheide et al.*, 2006]. The annual variation of the zonal wind of the DE3 tide is consistent with the measurements of the peak temperature of the DE3 tide at 110–116 km near September from TIMED/SABER [*Forbes et al.*, 2008; *Kil et al.*, 2008]. The annual variations of the amplitude of the wave-4 components in the vertical drift and density observed by ROCSAT-1 are consistent with the annual variation of the DE3-tide amplitude. The similar annual variation of the wave-4 component in the model ionosphere demonstrates the dominant role of the vertical drift in the formation of the wave-4 density structure. Therefore, the DE3 tide, vertical drift, and wave-4 density structure are closely linked with each other.

[13] Figure 5 shows the local time and longitudinal variations of the wave-4 components in the ROCSAT-1 vertical drift (top) and density (bottom), and the GIP density (middle) in September. The local time evolution of the

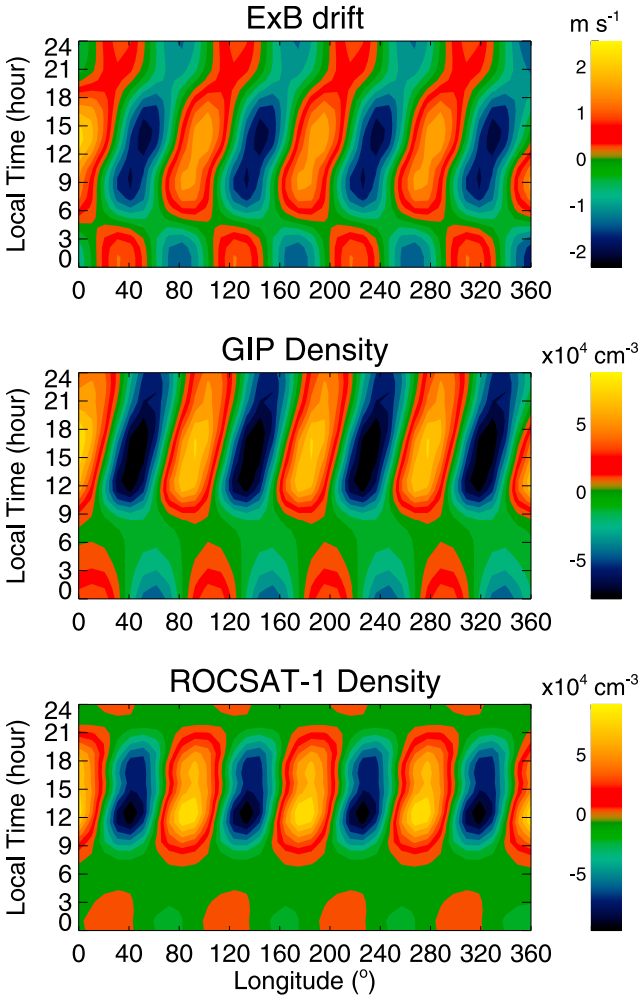

Figure 5. The local time and longitude variations of the wave-4 components in September: (top) the ROCSAT-1 vertical **E** × **B** drift at the magnetic equator, (middle) the GIP density, and (bottom) the ROCSAT-1 density.

wave-4 components further supports the causal link of the model density structure and the vertical drift with the DE3 tide. The wave-4 component in ROCSAT-1 vertical drifts emerges with sunrise and then shifts eastward in local time. The eastward shift is about 30° in longitude between 0600–1800 LT. The results from the GIP density show a similar eastward shift but the emergence of the wave-4 density structure occurs a few hours later than that in the vertical drift. A similar but somewhat smaller shift can be also seen in the ROCSAT-1 density in Figure 5 (bottom). A purely DE3 component of the drift or density would have a constant amplitude throughout the day, and would shift eastward by 45° in 12 h, more than what occurs during the day time for the parameters in Figure 5. On the other hand, a purely stationary wave number-4 feature would not shift at all as local time progresses at a fixed longitude, and would produce vertical stripes in Figure 5. We do not expect the temporal and spatial Fourier components of vertical drift and electron density to match one to one the components of the causative tides, because the ionospheric dynamo that generates the electric fields is influenced by longitudinal variations of the geomagnetic field and diurnal variations of the ionospheric conductivity, which will interact with the tides to produce other Fourier components. For example, the rapid change of the vertical drift before sunrise may be related to strong conductivity gradients at those local times. Nevertheless, we would expect a DE3 tide to tend to imprint an eastward progression of phase with local time on both the drift and electron density, as observed. The wave-4 component in the GIP density persists into the night, in agreement with the wave-4 component in the input vertical drift. However, the wave-4 component in the ROCSAT-1 density has a significant amplitude only during the day. At night, the PRE and/or neutral wind may significantly modify the daytime wave-4 density structure and the wave-4 component has a smaller amplitude in the real ionosphere than in the model ionosphere. These results indicate that the wave-4 component of the vertical **E** × **B** drift dominates the plasma density more at day than at night. The PRE and wind effect on the wave-4 density structure will be investigated in the future.

[14] The amplitude of the DE3 temperature at 110 km observed from TIMED/SABER during 20 July–20 September 2002 shows an eastward shift of the locations of the temperature crests with local time [*Forbes et al.*, 2006]. A similar phenomenon was observed in the wave-4 structure of the total electron content (TEC) produced using the global positioning system TEC maps during 1998–2007 [*Wan et al.*, 2008] and in the wave-4 component of the equatorial electrojet [*Lühr et al.*, 2008]. Our results are consistent with these previous studies. The relation between the DE3 temperature at 110 km observed by *Forbes et al.* [2006] and the vertical drift generated by DE3 winds through *E* region dynamo action is not simple, and so we do not attempt to compare the longitudinal displacement of the crest locations of the vertical drift with those of the DE3 temperature. The eastward shift of density can be different from that of vertical drift because the response of the density to the vertical drift is cumulative rather than instantaneous. Therefore, the wave-4 density features lag those of the vertical drift. The correlations between the amplitudes and phases of the vertical drift and the DE3 temperature still need to be investigated by modeling the dynamo effects of the DE3 tide.

[15] Since the wave-4 pattern is periodic in longitude, we select the data shown in Figure 5 for one cycle, between 60°E and 150°E longitude, and examine the annual variation. Figure 6 shows the annual variation of the ROCSAT-1 vertical drift (top) and density (bottom) and the GIP density (middle). As we have shown in Figure 4, the wave-4 amplitudes of the vertical drift and density are most pronounced in July–October. The eastward shift of the wave-4 component with local time is also observed mostly during these months. Comparison of the maps between May–June and September–October shows that the longitude of the wave-4 peak does not change much in these months. Verification of this property in the DE3 tide may further support the link of the ionospheric wave-4 structure with the DE3 tide. Although the GIP model is global, the current version solves all the equations in two dimensions in meridional planes, without longitudinal interaction. The effects of westward drift during the day, up to 60 m/s, and eastward drift at night, up to 150 m/s [*Fejer et al.*, 1991], are not presently included. Interacting with a zonal wave

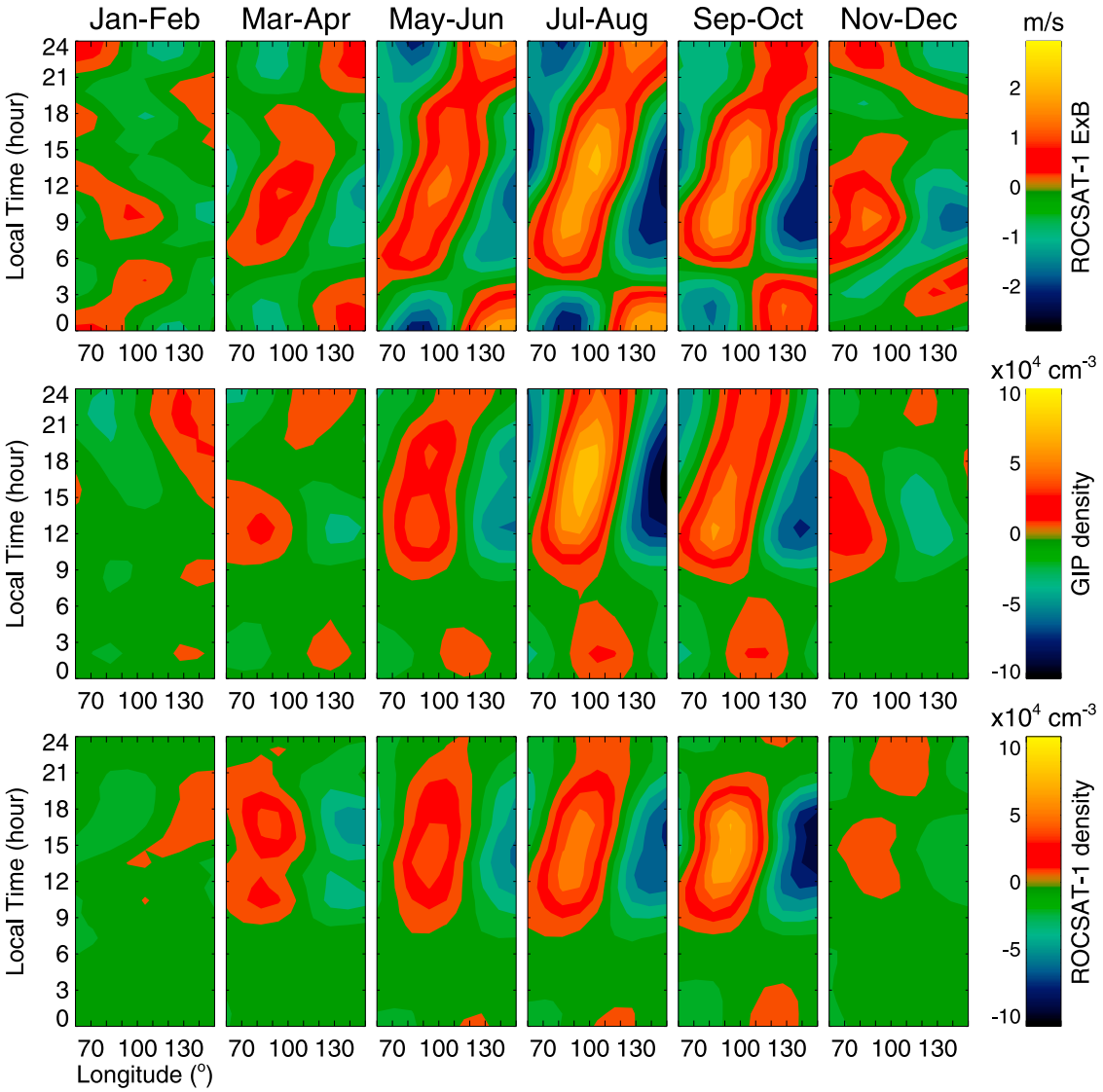

Figure 6. Annual, local time, and longitude variations of the amplitude of the wave-4 components. Figure 6 has the same format as Figure 5. Since the same pattern repeats, we present only the data between longitudes 60°E and 150°E.

number 3 feature like the DE3 tidal perturbation, a zonal ion drift u_i, if acting alone, would modulate the plasma density on a time scale of about $R_E/(3u_i)$, at least 9 h at day and at least 4 h at night, where R_E is the radius of the Earth. Diffusion, vertical transport, production, and/or loss are usually much more important on such time scales, justifying the neglect of zonal transport in a first approximation. In the future, however, inclusion of zonal drifts in the GIP model is desirable to rigorously evaluate their effect on the local time shift of the wave-4 structure.

5. Conclusions

[16] We demonstrate the three-dimensional electron density simulated by the GIP model, when driven by the empirical vertical **E** × **B** drift model based on the ROCSAT-1 data, together with empirical models of neutral wind and thermospheric parameters, reproduces reasonably well the three-dimensional electron density in the ionosphere. The simulations have allowed us to investigate the causal link of the longitudinal wave-4 density structure with the vertical drift in the low-latitude *F* region. The simulations verify that the annual and local time variations of the longitudinal structure in ionospheric density are controlled by the vertical **E** × **B** drifts. The peak amplitudes of the wave-4 component in the observed vertical drift and density occur during July–September. During these months the wave-4 components in the vertical drift and density show an eastward shift with increasing local time. The GIP model results show good agreement with these observations. Since the DE3 tide observed around 110 km altitude shows similar annual and local time variations as the *F* region vertical drifts and densities, our results provide strong evidence for the connection among the DE3 tide, vertical drift, and wave-4 density structure.

[17] **Acknowledgments.** T. W. Fang is supported by a NCAR/HAO Newkirk Graduate Research Fellowship and the project of the National Central University granted by National Science Council of Taiwan. The

National Center for Atmospheric Research is sponsored by the National Science Foundation. This work was supported in part by the CEDAR program. H. Kil acknowledges support from NASA grant NNX08AF32G.

[18] Wolfgang Baumjohann thanks Joseph Huba and two other reviewers for their assistance in evaluating this paper.

References

Anderson, D. N. (1973), Theoretical study of the ionospheric *F* region equatorial anomaly—I, *Planet. Space Sci.*, *21*(3), 409–419, doi:10.1016/0032-0633(73)90040-8.

Bailey, G. J., and N. Balan (1996), A low-latitude ionosphere-plasmasphere model, in *STEP Handbook on Ionospheric Models*, edited by R. W. Schunk, pp. 173–206, Utah State Univ., Logan.

Drob, D. P., et al. (2008), An empirical model of the Earth's horizontal wind fields: HWM07, *J. Geophys. Res.*, *113*, A12304, doi:10.1029/2008JA013668.

England, S. L., S. Maus, T. J. Immel, and S. B. Mende (2006), Longitudinal variation of the E-region electric fields caused by atmospheric tides, *Geophys. Res. Lett.*, *33*, L21105, doi:10.1029/2006GL027465.

Fejer, B. G., E. R. de Paula, S. A. González, and R. F. Woodman (1991), Average vertical and zonal F region plasma drifts over Jicamarca, *J. Geophys. Res.*, *96*(A8), 13,901–13,906, doi:10.1029/91JA01171.

Forbes, J. M., X. Zhang, E. R. Talaat, and W. Ward (2003), Nonmigrating diurnal tides in the thermosphere, *J. Geophys. Res.*, *108*(A1), 1033, doi:10.1029/2002JA009262.

Forbes, J. M., J. Russell, S. Miyahara, X. Zhang, S. Palo, M. Mlynczak, C. J. Mertens, and M. E. Hagan (2006), Troposphere-thermosphere tidal coupling as measured by the SABER instrument on TIMED during July–September 2002, *J. Geophys. Res.*, *111*, A10S06, doi:10.1029/2005JA011492.

Forbes, J. M., X. Zhang, S. Palo, J. Russell, C. J. Mertens, and M. Mlynczak (2008), Tidal variability in the ionospheric dynamo region, *J. Geophys. Res.*, *113*, A02310, doi:10.1029/2007JA012737.

Fuller-Rowell, T. J., et al. (2008), Impact of terrestrial weather on the upper atmosphere, *Geophys. Res. Lett.*, *35*, L09808, doi:10.1029/2007GL032911.

Hagan, M. E., A. Maute, R. G. Roble, A. D. Richmond, T. J. Immel, and S. L. England (2007), Connections between deep tropical clouds and the Earth's ionosphere, *Geophys. Res. Lett.*, *34*, L20109, doi:10.1029/2007GL030142.

Hanson, W. B., and R. J. Moffett (1966), Ionization transport effects in the equatorial F region, *J. Geophys. Res.*, *71*, 5559–5572.

Hartman, W. A., and R. A. Heelis (2007), Longitudinal variations in the equatorial vertical drift in the topside ionosphere, *J. Geophys. Res.*, *112*, A03305, doi:10.1029/2006JA011773.

Huba, J. D., G. Joyce, and J. A. Fedder (2000), Sami2 is Another Model of the Ionosphere (SAMI2): A new low-latitude ionosphere model, *J. Geophys. Res.*, *105*, 23,035–23,053, doi:10.1029/2000JA000035.

Immel, T. J., E. Sagawa, S. L. England, S. B. Henderson, M. E. Hagan, S. B. Mende, H. U. Frey, C. M. Swenson, and L. J. Paxton (2006), Control of equatorial ionospheric morphology by atmospheric tides, *Geophys. Res. Lett.*, *33*, L15108, doi:10.1029/2006GL026161.

Immel, T. J., S. B. Mende, M. E. Hagan, P. M. Kintner, and S. L. England (2009), Evidence of tropospheric effects on the ionosphere, *Eos Trans. AGU*, *90*(9), 69–70, doi:10.1029/2009EO090001.

Jin, H., Y. Miyoshi, H. Fujiwara, and H. Shinagawa (2008), Electrodynamics of the formation of ionospheric wave number 4 longitudinal structure, *J. Geophys. Res.*, *113*, A09307, doi:10.1029/2008JA013301.

Kil, H., R. DeMajistre, L. J. Paxton, and Y. Zhang (2006), Nighttime *F* region morphology in the low and middle latitudes seen from DMSP F15 and TIMED/GUVI, *J. Atmos. Sol. Terr. Phys.*, *68*, 1672–1681, doi:10.1016/j.jastp.2006.05.024.

Kil, H., S.-J. Oh, M. C. Kelley, L. J. Paxton, S. L. England, E. Talaat, K.-W. Min, and S.-Y. Su (2007), Longitudinal structure of the vertical $\mathbf{E} \times \mathbf{B}$ drift and ion density seen from ROCSAT-1, *Geophys. Res. Lett.*, *34*, L14110, doi:10.1029/2007GL030018.

Kil, H., E. R. Talaat, S.-J. Oh, L. J. Paxton, S. L. England, and S.-J. Su (2008), Wave structures of the plasma density and vertical $\mathbf{E} \times \mathbf{B}$ drift in low-latitude *F* region, *J. Geophys. Res.*, *113*, A09312, doi:10.1029/2008JA013106.

Kil, H., S.-J. Oh, L. J. Paxton, and T.-W. Fang (2009a), High-resolution vertical $\mathbf{E} \times \mathbf{B}$ drift model derived from ROCSAT-1 data, *J. Geophys. Res.*, *114*, A10314, doi:10.1029/2009JA014324.

Kil, H., L. J. Paxton, and S.-J. Oh (2009b), Global bubble distribution seen from ROCSAT-1 and its association with the evening prereversal enhancement, *J. Geophys. Res.*, *114*, A06307, doi:10.1029/2008JA013672.

Lin, C. H., W. Wang, M. E. Hagan, C. C. Hsiao, T. J. Immel, M. L. Hsu, J. Y. Liu, L. J. Paxton, T. W. Fang, and C. H. Liu (2007a), Plausible effect of atmospheric tides on the equatorial ionosphere observed by the FORMOSAT-3/COSMIC: Three-dimensional electron density structures, *Geophys. Res. Lett.*, *34*, L11112, doi:10.1029/2007GL029265.

Lin, C. H., C. C. Hsiao, J. Y. Liu, and C. H. Liu (2007b), Longitudinal structure of the equatorial ionosphere: Time evolution of the four-peaked EIA structure, *J. Geophys. Res.*, *112*, A12305, doi:10.1029/2007JA012455.

Lin, C. H., J. Y. Liu, T. W. Fang, P. Y. Chang, H. F. Tsai, C. H. Chen, and C. C. Hsiao (2007c), Motions of the equatorial ionization anomaly crests imaged by FORMOSAT-3/COSMIC, *Geophys. Res. Lett.*, *34*, L19101, doi:10.1029/2007GL030741.

Liu, H., and S. Watanabe (2008), Seasonal variation of the longitudinal structure of the equatorial ionosphere: Does it reflect tidal influences from below?, *J. Geophys. Res.*, *113*, A08315, doi:10.1029/2008JA013027.

Lühr, H., K. Häusler, and C. Stolle (2007), Longitudinal variation of *F* region electron density and thermospheric zonal wind caused by atmospheric tides, *Geophys. Res. Lett.*, *34*, L16102, doi:10.1029/2007GL030639.

Lühr, H., M. Rother, K. Hausler, P. Alken, and S. Maus (2008), Influence of nonmigrating tides on the longitudinal variation of the equatorial electrojet, *J. Geophys. Res.*, *113*, A08313, doi:10.1029/2008JA013064.

Millward, G. H., I. C. F. Muller-Wodarg, A. D. Aylward, T. J. Fuller-Rowell, A. D. Richmond, and R. J. Moffett (2001), An investigation into the influence of tidal forcing on *F* region equatorial vertical ion drift using a global ionosphere-thermosphere model with coupled electrodynamics, *J. Geophys. Res.*, *106*, 24,733–24,744, doi:10.1029/2000JA000342.

Millward, G. H., A. D. Richmond, T. J. Fuller-Rowell, and A. D. Aylward (2007), Modeling the effect of changes in the terrestrial magnetic field on the climatology of the mid- and low-latitude ionosphere, *Eos Trans. AGU*, *88*(52), Fall Meet. Suppl., Abstract SA21B-08.

Oberheide, J., Q. Wu, T. L. Killeen, M. E. Hagan, and R. G. Roble (2006), Diurnal nonmigrating tides from TIMED Doppler Interferometer wind data: Monthly climatologies and seasonal variations, *J. Geophys. Res.*, *111*, A10S03, doi:10.1029/2005JA011491.

Oh, S.-J., H. Kil, W.-T. Kim, L. J. Paxton, and Y. H. Kim (2008), The role of the vertical $\mathbf{E} \times \mathbf{B}$ drift for the formation of the longitudinal plasma density structure in the low-latitude *F* region, *Ann. Geophys.*, *26*, 2061–2067.

Picone, J. M., A. E. Hedin, D. P. Drob, and A. C. Aikin (2002), NRLMSISE-00 empirical model of the atmosphere: Statistical comparisons and scientific issues, *J. Geophys. Res.*, *107*(A12), 1468, doi:10.1029/2002JA009430.

Richmond, A. D. (1995), Ionospheric electrodynamics using magnetic apex coordinates, *J. Geomagn. Geoelectr.*, *47*, 191–212.

Scherliess, L., and B. G. Fejer (1999), Radar and satellite global equatorial *F* region vertical drift model, *J. Geophys. Res.*, *104*(A4), 6829–6842, doi:10.1029/1999JA900025.

Scherliess, L., D. C. Thompson, and R. W. Schunk (2008), Longitudinal variability of low-latitude total electron content: Tidal influences, *J. Geophys. Res.*, *113*, A01311, doi:10.1029/2007JA012480.

Stolle, C., C. Manoj, H. Lühr, S. Maus, and P. Alken (2008), Estimating the daytime Equatorial Ionization Anomaly strength from electric field proxies, *J. Geophys. Res.*, *113*, A09310, doi:10.1029/2007JA012781.

Torr, M. R., and D. G. Torr (1982), The role of metastable species in the thermosphere, *Rev. Geophys. Space Phys.*, *20*(1), 91–144, doi:10.1029/RG020i001p00091.

Torr, M. R., and D. G. Torr (1985), Ionization frequencies for solar cycle 21: Revised, *J. Geophys. Res.*, *90*, 6675–6678, doi:10.1029/JA090iA07p06675.

Wan, W., L. Liu, X. Pi, M.-L. Zhang, B. Ning, J. Xiong, and F. Ding (2008), Wavenumber-4 patterns of the total electron content over the low latitude ionosphere, *Geophys. Res. Lett.*, *35*, L12104, doi:10.1029/2008GL033755.

Yeh, H. C., S.-Y. Su, R. A. Heelis, and J. M. Wu (1999), The ROCSAT-1 IPEI preliminary results: Vertical ion drift statistics, *Terr. Atmos. Oceanic Sci.*, *10*, 805–820.

T.-W. Fang and A. D. Richmond, High Altitude Observatory, National Center for Atmospheric Research, P.O. Box 3000, Boulder, CO 80307-3000, USA. (twfang@ucar.edu; richmond@ucar.edu)

H. Kil, Johns Hopkins University Applied Physics Laboratory, 11100 Johns Hopkins Road, Laurel, MD 20723, USA. (hyosub.kil@jhuapl.edu)

J.-Y. Liu, Institute of Space Science, National Central University, No. 300, Joongda Road, Jhongli City, Taoyuan County 32001, Taiwan. (jyliu@jupiter.ss.ncu.edu.tw)

G. Millward, Laboratory for Atmospheric and Space Physics, University of Colorado at Boulder, 1234 Innovation Drive, Boulder, CO 80303-7814, USA. (george.millward@noaa.gov)

S.-J. Oh, Space Environment Laboratory, Inc., 5th Floor, Jin-Young Building, 66-3 Non-Hyun Dong, Gang-Nam Gu, Seoul, South Korea. (oh@spweather.com)